Calculated and Measured Reflectivity of ZnTe and ZnSe†

JOHN P. WALTER* AND MARVIN L. COHEN
Department of Physics and Inorganic Materials Research Division, University of California, Berkeley, California 94720

AND

Y. PETROFF AND M. BALKANSKI
Laboratoire de Physique des Solides de la Faculté des Sciences de Paris, France and Equipe de Recherche associée au Centre National de la Recherche Scientifique, Paris, France

(Received 14 November 1969)

Reflectivity spectra of ZnTe and ZnSe are studied experimentally and theoretically. The measurements are made at 15 and 300°K, and the theoretical calculations are done at an assumed temperature of 300°K. Spin-orbit interactions are included in the empirical pseudopotential calculation of the electronic band structures for both ZnTe and ZnSe. The imaginary part of the frequency-dependent dielectric function, the reflectivity, and the derivative of the reflectivity are calculated. In addition, a direct comparison of the measured and calculated reflectivity is made. The calculated derivative of the reflectivity is compared with thermo-reflectance data. The electronic transitions causing the reflectivity peaks are identified.

I. INTRODUCTION

DETAILED reflectivity data for cubic ZnTe and ZnSe at 15 and 300°K have been obtained. The experimental procedures are described in the next section and the results appear in Figs. 3, 7, and 9.

The relativistic electronic energy band structures for ZnTe and ZnSe are calculated using the empirical pseudopotential method,[1] modified by Bloom and Bergstresser to include spin-orbit coupling.[2] In addition, we have calculated the imaginary part of the frequency-dependent dielectric function $\epsilon_2(\omega)$, the reflectivity $R(\omega)$, and the logarithmic derivative of the reflectivity $R'(\omega)/R(\omega)$. The calculated reflectivity is compared directly with the measured reflectivity at 300°K.

Pseudopotential form factors for these crystals were originally obtained by Cohen and Bergstresser[1] by comparison of their band structure with the existing optical data.[1,3,4] New measurements of the optical properties[5–7] have been made since that time. The results of these measurements and a direct comparison between the experimental and the theoretical $R(\omega)$ were used to make small adjustments in the form factors. The spin-orbit form factor was determined by adjusting the valence band splitting at Γ_{15} to agree with the experimental value.

We have made a critical point analysis to identify the optical structure in terms of interband transitions. The symmetries and positions in energy of the important critical points have been determined and their contributions to $\epsilon_2(\omega)$ and $R(\omega)$ have been investigated.

A comparison between theory and experiment shows good agreement for both the reflectivity and the logarithmic derivative of the reflectivity. The latter is compared only with thermoreflectance data[7] and not with electroreflectance data. The reason for this restriction is that electroreflectance involves a more complicated variation of the reflectivity, and consequently a simple derivative of the type we have calculated is more appropriate for comparison with thermoreflectance data. Wavelength modulation spectra would provide the best comparison, but the spectra for ZnTe and ZnSe are unavailable.

The temperature shifts of the reflectivity peaks are discussed in terms of the Debye-Waller effect and the thermal expansion of the lattice.[8] The sharpening of the reflectivity peaks at low temperature is discussed in connection with exciton effects.

Finally, we discuss possible effects of including indirect transitions at energies greater than twice the fundamental gap. The result is to smooth $\epsilon_2(\omega)$ at higher energies and to cause $R(\omega)$ to agree more closely with experiment at high energies.

II. EXPERIMENT

The reflectivity measurements are made with a 218 MacPherson monochromator, fitted with a special low-temperature reflectometer.[9] The light source is a Tonaku hydrogen-gas capillary discharge lamp. The samples are cleaved in air along the (110) plane and mounted in a cryostat, which is then evacuated to a pressure of 5×10^{-9} mm Hg by an ionic pump in conjunction with a liquid-helium trap. The light enters the cryostat through a lithium-fluoride window, allow-

† Supported in part by the National Science Foundation.
* National Science Foundation Graduate Fellow.
[1] M. L. Cohen and T. K. Bergstresser, Phys. Rev. **141**, 789 (1966), and references therein.
[2] S. Bloom and T. K. Bergstresser, Solid State Commun. 6, 465 (1968).
[3] M. Cardona and D. L. Greenaway, Phys. Rev. **131**, 98 (1963).
[4] M. Aven, D. T. F. Marple, and B. Segall, J. Appl. Phys. Suppl. **32**, 2261 (1961).
[5] Y. Petroff, M. Balkanski, J. P. Walter, and M. L. Cohen, Solid State Commun. **7**, 459 (1969).
[6] M. Cardona, K. L. Shaklee, and F. H. Pollack, Phys. Rev. **154**, 696 (1967).
[7] E. Matatagui, A. G. Thompson, and M. Cardona, Phys. Rev. **176**, 950 (1968).
[8] J. P. Walter, R. R. L. Zucca, M. L. Cohen, and Y. R. Shen, Phys. Rev. Letters **24**, 102 (1970).
[9] Y. Petroff, R. Pinehaun, and J. Dayneoun (unpublished).

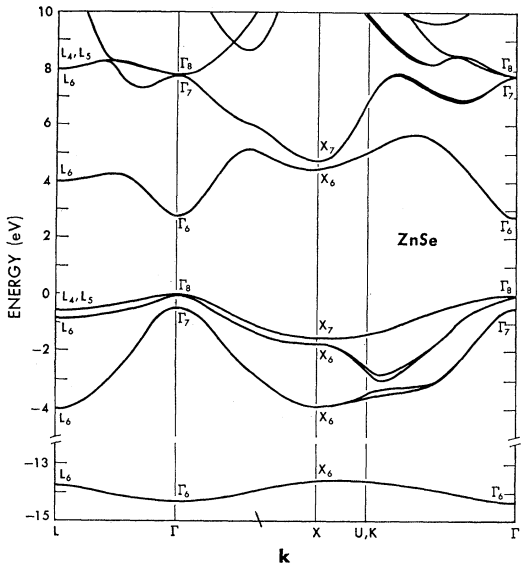

FIG. 1. Band structure of ZnTe along the principal symmetry directions.

ing measurements up to 11 eV. The cryostat is designed to allow measurements from liquid-helium temperature to room temperature. The optical system allows measurements to be made on a sample surface as small as 3×3 mm^2.

The results of the reflectivity measurements for ZnTe and ZnSe appear in Figs. 3 and 7 (300°K) and in Fig. 9 (15°K).

A. Calculations

The empirical pseudopotential method involves adjusting pseudopotential form factors to achieve good agreement with experimental results for the principal optical transitions. These form factors are then used to determine the electronic energy bands on a fine mesh of points in the Brillouin zone.

The initial calculations begin with the spin-free pseudopotential Hamiltonian

$$\mathcal{H}=\frac{-\hbar^2}{2m}\nabla^2+V(\mathbf{r}). \tag{1}$$

The pseudopotential form factors are adjusted by the procedure described in Ref. 10. Only slight over-all adjustments are necessary, as can be seen from Table I. $\epsilon_2(\omega)$ is shown for the spin-free case in Figs. 2 and 6.

TABLE I. Comparison of the ZnTe and ZnSe form factors (in Ry) used in the present work (on top) with those used in Ref. 1.

	$V^S(3)$	$V^S(8)$	$V^S(11)$	$V^A(3)$	$V^A(4)$	$V^A(11)$	Metallic spin-orbit
ZnTe	−0.217	−0.018	0.069	0.116	0.073	−0.011	0.0010
	−0.22	0.00	0.05	0.13	0.10	0.01	···
ZnSe	−0.213	−0.011	0.067	0.203	0.107	0.015	0.0006
	−0.23	0.01	0.06	0.18	0.12	0.03	···

TABLE II. Calculated spin-orbit splitting (in eV) in the single-group notation for cubic ZnTe and ZnSe. The spin-orbit parameter was determined by adjusting the Γ_{15V} splitting to agree with experiment.

	ZnTe	ZnSe
Γ_{15V}	0.92	0.45
L_{3V}	0.58	0.29
X_{5V}	0.46	0.25
Γ_{15C}	0.16	0.05
L_{3C}	0.07	0.02

In adding spin-orbit interactions, we use the model introduced by Weisz[11] for white tin and modified by Bloom and Bergstresser[2] for grey tin, CdTe, and InSb. The Hamiltonian matrix element in the plane-wave representation is

$$\begin{aligned}\langle\mathbf{k}+\mathbf{G}',s'|\mathcal{H}|\mathbf{k}+\mathbf{G},s\rangle&=(2m)^{-1}|\mathbf{k}+\mathbf{G}|^2\delta_{\mathbf{G}',\mathbf{G}}\delta_{s',s}\\&+S^S(\mathbf{G}-\mathbf{G}')[V^S(|\mathbf{G}-\mathbf{G}'|^2)\delta_{s',s}-i\lambda^S(\hat{G}'\times\hat{G})\cdot\boldsymbol{\sigma}_{s',s}]\\&+iS^A(\mathbf{G}-\mathbf{G}')[V^A(|\mathbf{G}-\mathbf{G}'|^2)\delta_{s',s}\\&\qquad-i\lambda^A(\hat{G}'\times\hat{G})\cdot\boldsymbol{\sigma}_{s',s}].\end{aligned}$$

S^S and S^A are the symmetric and antisymmetric structure factors and V^S and V^A are the symmetric and antisymmetric pseudopotentials (see Ref. 1). λ^S and λ^A are defined as follows:

$$\lambda^S=\tfrac{1}{2}(\lambda_1+\lambda_2),\quad \lambda^A=\tfrac{1}{2}(\lambda_1-\lambda_2),$$
$$\lambda_1=\mu B_{nl}(G)B_{nl}(G'),\quad\text{and}\quad \lambda_2=\alpha\mu B_{nl}(G)B_{nl}(G'),$$

where λ_1 and λ_2 are the metallic and nonmetallic contributions, the B_{nl} are the orthogonalization integrals for the metal in λ_1 and for the nonmetal in λ_2, μ is the spin-orbit parameter, and α is the ratio of the nonmetallic contribution to the metallic contribution for $\mathbf{G}=\mathbf{G}'=0$.[12] The B_{nl} are defined as follows:

$$B_{nl}(k)=C\int_0^\infty j_l(kr)R_{nl}(r)r^2dr,$$

where C is determined by the condition

$$\lim_{k\to0}k^{-l}B_{nl}(k)=1,$$

and the R_{nl} are tabulated Hartree-Fock-Slater orbitals.[12] In our calculation, nl is $3p$ for Zn and Se and $4p$ for Te. The d contributions are neglected, as well as contributions from lower-lying p states.

The spin-orbit parameter μ is varied to give the correct splitting of the valence band at Γ_{15}. This splitting is denoted by Δ_0. The experimental values of Δ_0 are

[10] J. P. Walter and M. L. Cohen, Phys. Rev. **183**, 763 (1969).

[11] G. Weisz, Phys. Rev. **149**, 504 (1966).

[12] F. Herman and S. Skillman, *Atomic Structure Calculations* (Prentice-Hall, Inc., Englewood Cliffs, N. J., 1966).

[13] P. Eckelt, Solid State Commun. **6**, 489 (1968), and references therein.

TABLE III. Theoretical and experimental reflectivity structure at 300°K and their identifications, including the location in the Brillouin zone, energy, and symmetry of the calculated critical points for ZnTe.

Reflectivity structure (eV)		Associated transitions		
Theory	Experiment	Location in zone	Symmetry	Transition energy (eV)
2.20	···	Γ_8-Γ_6	M_0	2.21
···	···	Γ_7-Γ_6	M_0	3.14
3.70	3.58	L_4, L_5-L_6	M_0	3.45
		Λ(8-10) (0.3,0.3,0.3)	M_1	3.64
4.15	3.99	L_6-L_6	M_0	4.03
4.30	4.18	Λ(6-10) (0.3,0.3,0.3)	M_1	4.21
4.65	···	X_7-X_6	M_0	4.59
4.95	4.92	Δ(8-10) (0.5,0.,0.)	M_1	4.93
5.25	···	K(8-9)	M_0	5.26
5.45	5.51	K(7-10)	M_0	5.35
		Δ(6-10) (0.5,0.,0.)	M_1	5.39
		Σ(7-10) (0.6,0.6,0.)	M_2	5.50
5.85	5.9	Δ(8-12) (0.6,0.,0.)	M_1	5.67
6.10	···	Δ(6-12) (0.6,0.,0.)	M_2	6.13
6.85	6.87	Vol. effect (7-12) and (8-11) from region around (0.6,0.4,0.3)	···	6.72
7.65	7.58	Vol. effect (6-11) (0.6,0.4,0.3)	···	7.28
		Vol. effect (5-12) (0.6,0.4,0.3)	···	7.47
		Λ(6-13) (0.4,0.4,0.4)	M_1	7.57

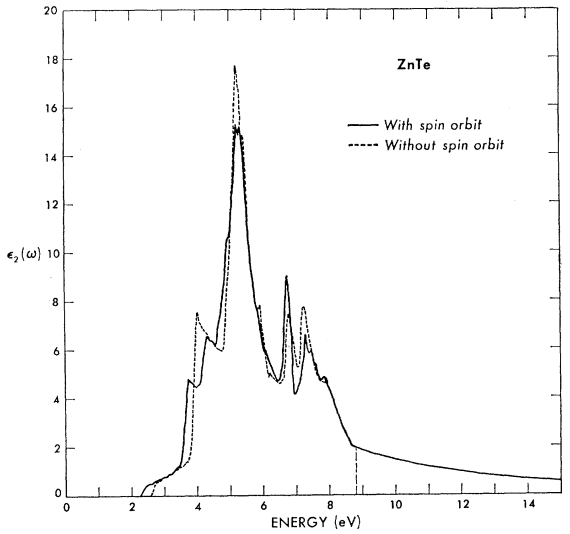

FIG. 2. Theoretical $\epsilon_2(\omega)$ for ZnTe, with and without spin-orbit contributions. The tail function begins at 8.83 eV.

0.93 eV for ZnTe and 0.45 eV for ZnSe.[1,13] The spin-orbit splittings we obtain are shown in Table II.

The calculation of $\epsilon_2(\omega)$, the addition of the tail function, and the calculation of $R(\omega)$ are all performed as described in Ref. 10.

B. Results

The band structures in the principal symmetry directions and graphs of selected optical functions are shown in Figs. 1–8. Table I presents a comparison of Cohen-Bergstresser form factors and those derived in this work. Table II presents the important spin-orbit splittings. Tables III and IV tabulate the important critical points for these two compounds.

ZnTe. The threshold in $\epsilon_2(\omega)$ at 2.21 eV is caused by Γ_8-Γ_6 transitions. Γ_7-Γ_6 transitions at 3.14 eV cause a slight rise in ϵ_2, but it is of the same magnitude as fluctuations at 2.60 eV and 3.25 eV. The start of the rise at 3.45 eV is caused by L_4,L_5-$L_6(M_0)$ transitions at 3.45 eV. The first peak at 3.7 eV corresponds to Λ(8-10)(M_1) transitions[14] at 3.64 eV. The rise and peak in the 4.05–4.27-eV region correspond to L_6-$L_6(M_0)$ transitions at 4.03 eV and Λ(6-10)M_1 transitions at 4.21 eV. The small bulge at 4.58 eV is caused by X_7-$X_6(M_0)$ transitions at 4.59 eV. The shoulder at 4.92 eV is caused by Δ(8-10)M_1 transitions at 4.93 eV. Another small bulge at 5.10 eV is caused by X_6-$X_6(M_0)$ transitions at 5.05 eV. The main peak is slightly split into two peaks at 5.22 and 5.32 eV and is caused chiefly by transitions (7-9), (7-10), (8-9), and (8-10) along the Σ and Δ directions. In particular the peak at 5.22 eV is caused by (8-9) transitions in a volume near K. The peak at 5.32 eV is caused by (7-10) transitions in a volume near K, with Δ(6-10)(M_1) transitions at 5.39 eV and Σ(7-10)(M_2) transitions at 5.50 eV contributing to a smaller extent. The shoulder at 6.07 eV is caused by Δ(6-12)(M_2) transitions at 6.13 eV. The

[14] In this notation, the bands are numbered consecutively, with the highest energy valence band numbered 8. The bands are doubly degenerate in the Δ and Λ directions, except for an extremely small splitting at L_4, L_5. Accordingly, a label (8-10) in one of these directions also includes transitions (7-9), (7-10), and (8-9). The proper group notation is used only where such labeling is unambiguous.

TABLE IV. Theoretical and experimental reflectivity structure at 300°K and their identifications, including the location in the Brillouin zone, energy, and symmetry of the calculated critical points for ZnSe.

Reflectivity structure (eV)		Associated transitions		
Theory	Experiment	Location in zone	Symmetry	Transition energy (eV)
2.80	···	Γ_8-Γ_6	M_0	2.77
3.20	···	Γ_7-Γ_6	M_0	3.22
4.72	4.75	L_4, L_5-L_6	M_0	4.53
		Λ(8-10) (0.3,0.3,0.3)	M_1	4.64
5.00	5.05	L_6-L_6	M_0	4.82
		Λ(6-10) (0.3,0.3,0.3)	M_1	4.94
5.97	6.00	X_7-X_6	M_0	5.92
6.20	···	Δ(8-10) (0.6,0.,0.)	M_1	6.11
6.47	6.50	Δ(6-10) (0.6,0.,0.) Comes chiefly from the sum of Δ(8-10), Σ(7-9), and Σ(8-10) transitions	M_1	6.37
6.62	6.63	Σ(7-9) and Σ(8-10), both at (0.6,0.6,0.)	M_2	6.62
7.10	7.15	Δ(8-12) (0.6,0.,0.)	M_1	7.02
7.42	7.60	Δ(6-12) (0.6,0.,0.)	M_1	7.28
7.67		Σ(6-12) (0.2,0.2,0.)	M_2	7.60
7.88	7.80	Γ_8-Γ_8	···	7.80
8.20	8.46	Vol. effect (8-12) and (7-11) (0.6,0.5,0.2)	···	8.13
8.50		L(8-12)	···	8.51
8.85	8.97	Vol. effect (5-12), (6-11), (5-11) and (6-12) (0.6,0.5,0.2)		8.80
		Λ(8-14) (0.3,0.3,0.3)		8.69

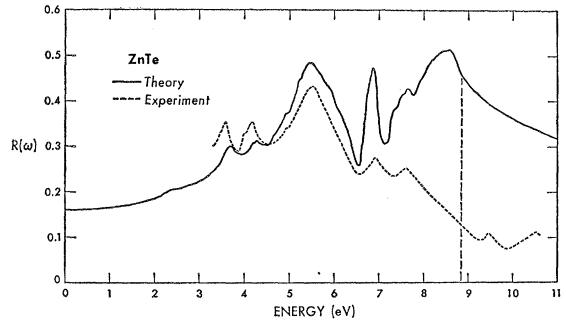

FIG. 3. Comparison of theoretical and experimental $R(\omega)$ for ZnTe at 300°K. The tail function begins at 8.83 eV.

peak at 6.72 eV is caused by (7-12) and (8-11) transitions, both located in a volume centered at (0.6,0.4,0.3) (units of $2\pi/a$). The peak at 7.28 eV is caused by (6-11) transitions in a volume centered at (0.6,0.4,0.3). The peak at 7.47 eV is caused by (5-12) transitions in a volume centered at (0.6,0.4,0.3). The shoulder at 7.57 eV is caused by Λ(6-13)(M_2) transitions at 7.57 eV. The peak at 7.82 eV is caused by (6-13) transitions in a volume centered at (0.5,0.3,0.1).

A comparison of $\epsilon_2(\omega)$ with and without spin-orbit contributions shows the principal consequences of "turning off" the spin-orbit interaction (Fig. 2). For the spin-free ϵ_2, the threshold occurs $\frac{1}{3}\Delta_0$ higher in energy. The two Λ peaks at 3.72 and 4.27 eV move together to form one Λ peak at 4.02 eV. The Δ transitions at 4.93 and 5.39 eV move together to form the main peak at 5.22 eV. The transitions near K move to 5.35 eV and the Σ transitions at 5.38 and 5.50 eV move to 5.48 eV to cause the shoulder at 5.42 eV. Δ transitions at 5.67 (barely discernible shoulder in the spin ϵ_2) and at 6.13 move together to form the peak at 6.78 eV. In addition, the bending of the bands when the interaction is turned off introduces a critical point in the Λ direction which contributes a major portion to the 6.78-eV peak.

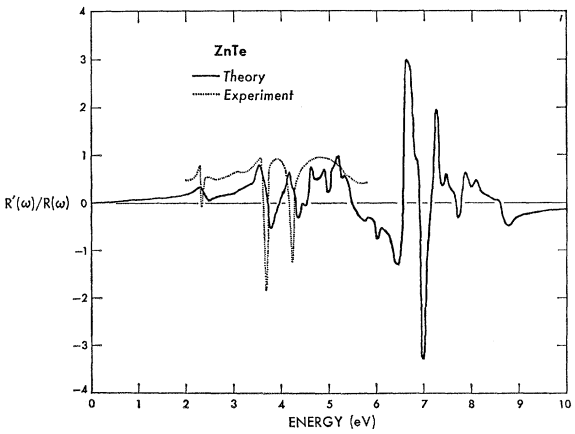

FIG. 4. Comparison for ZnTe of theoretical $R'(\omega)/R(\omega)$ with thermoreflectance measurements by Matatagui *et al.* (Ref. 7). The experimental measurements are multiplied by a constant scale factor.

The (6-11) and (5-12) transitions in the vicinity of (0.6,0.4,0.3) move together at 7.22 eV and the Λ transition at 7.57 eV also moves to 7.24 eV.

The experimental and theoretical reflectivity at 300°K appear in Fig. 3, and details of the reflectivity structure are shown in Table III. The theoretical Λ peak at 3.70 eV corresponds to the experimental peak at 3.58 eV. The second Λ peak at 4.30 eV corresponds to the experimental peak at 4.18 eV. A small shoulder appears on the low-energy side of the peak for both theory and experiment. The shoulder at 4.65 eV does not appear in the experimental reflectivity. The shoulder at 4.95 eV is caused by Δ(8-10) transitions and corresponds to the experimental shoulder at 4.92 eV. The shoulder at 5.25 eV does not appear in the experimental measurements 300°K. The main peak occurs at 5.45 eV for theory and at 5.51 eV for experiment. The experimental reflectivity from 5.6 to 6.5 eV is remarkably

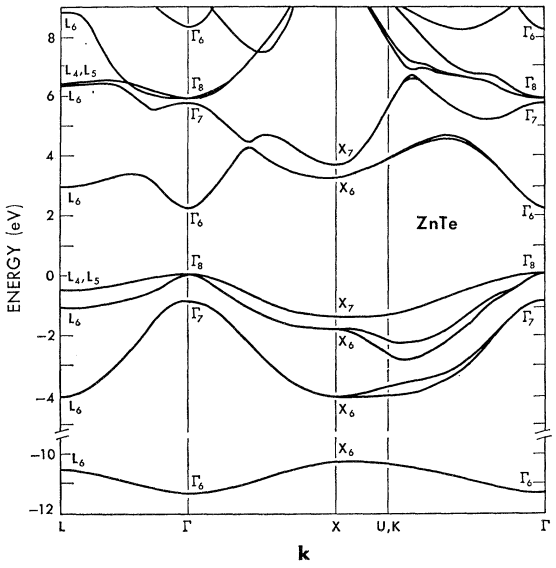

FIG. 5. Band structure for ZnSe along the principal symmetry directions.

linear, except for a practically imperceptible bulge at 5.9 eV. The calculated $R(\omega)$ has slight shoulders at 5.85 and 6.10 eV. The next peak occurs at 6.85 eV for theory and at 6.87 eV for experiment, but the two differ considerably in amplitude. The next peak occurs at 7.65 eV for theory and 7.58 eV for experiment. The theoretical $R(\omega)$ shows two shoulders at 7.35 and 7.55 eV which do not appear in the experiment. The last theoretical peak shows absolutely no correlation with experiment; it is caused by the steep negative slope of $\epsilon_2(\omega)$ in the region 7.9–8.6 eV. The amplitude of the theoretical $R(\omega)$ in this region is considerably greater than that of the experimental $R(\omega)$; this will be discussed in more detail later. However, the over-all agreement between experiment and theory, especially with regard to peak positioning, is good for ZnTe.

A comparison of $R'(\omega)/R(\omega)$ and thermoreflectance data appears in Fig. 4.

ZnSe. The threshold in $\epsilon_2(\omega)$ at 2.77 eV is caused by Γ_8-Γ_6 transitions. Γ_7-Γ_6 transitions at 3.22 eV cause a slight rise in ϵ_2. The start of the rise at 4.57 eV is caused by L_4, L_5-$L_6(M_0)$ transitions at 4.53 eV. The peak at 4.72 eV is caused by Λ(8-10)(M_1) transitions at 4.64 eV. The rise and peak in the 4.75- to 5.02-eV region correspond to L_6-$L_6(M_0)$ transitions at 4.82 eV and Λ(6-10)M_1 transitions at 4.94 eV. These are the two spin-orbit split Λ peaks. The start of the rise of the main peak is caused by X_7-$X_6(M_0)$ transitions at 5.92 eV. A small bulge at 6.2 eV corresponds to Δ(8-10)(M_1) transitions at 6.11 eV. The slight shoulder at 6.6 eV is caused by Σ(7-9) and Σ(8-10)(M_2) transitions at 6.62 eV. The sum of the Δ(8-10), Σ(7-9), and Σ(8-10) transitions, plus that of Δ(6-10) transitions at 6.37 eV, causes the main peak at 6.42 eV. The next two peaks are spin-orbit split Δ peaks; the one at 7.07 eV is caused

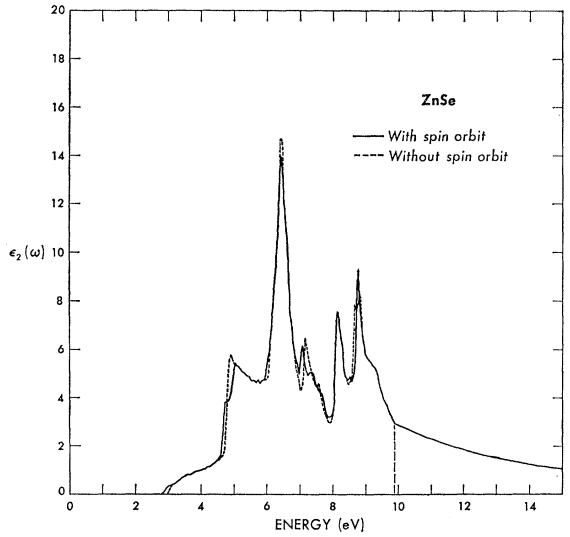

FIG. 6. Theoretical $\epsilon_2(\omega)$ for ZnSe, with and without spin-orbit contributions. The tail function begins at 9.93 eV.

by Δ(8-12)(M_1) transitions at 7.02 eV and the one at 7.32 eV is caused by Δ(6-12)(M_1) transitions at 7.28 eV. The shoulder at 7.63 eV is attributed to Σ(6-12)(M_2) transitions at 7.60 eV. The peak at 8.13 eV is caused by (8-12) and (7-11) transitions, both in a volume centered at (0.6,0.5,0.2). The small peak at 8.52 eV is attributed to L(8-12) transitions at 8.51 eV. The peak at 8.77 eV is caused by (5-12), (6-11), (5-11), and (6-12) transitions, all centered at (0.6,0.5,0.2). Λ(8-14) transitions at 8.69 eV also contribute. The shoulder at 9.27 eV is caused by (5-14) and (6-13) transitions from a volume centered at (0.5,0.2,0.1).

If the spin-orbit interaction is turned off (Fig. 6), the threshold for $\epsilon_2(\omega)$ occurs $\frac{1}{3}\Delta_0$ higher in energy. The two Λ peaks at 4.72 and 5.02 eV move together. The base of the main peak on its low-energy side becomes

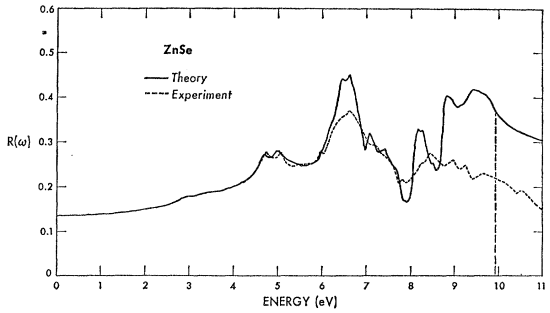

FIG. 7. Comparison of theoretical and experimental $R(\omega)$ for ZnSe at 300°K. The experimental results are due to Petroff and Balkanski (Ref. 5). The tail function begins at 9.93 eV.

narrower because of the bands at X are not as flat. The Δ(8-10) and Δ(6-10) transitions move together causing the main peak to become larger and also serving to narrow the base of the main peak on its low-energy side. The Δ(8-12) peak at 7.07 eV and the Δ(6-12) peak at 7.32 eV also move together. The strength of the Γ transitions at 7.9 eV becomes less because the bands are not as flat. Finally, the small L peak at 8.51 eV moves to a slightly higher energy at 8.65 eV.

The experimental and theoretical reflectivity at 300°K appear in Fig. 7, and details of the reflectivity structure are shown in Table IV. Excellent agreement exists between experiment and theory in the range 4.2 to 5.9 eV. The experimental peak at 6.0 eV corresponds to a slight bulge in the theoretical $R(\omega)$, which is caused by X_7-X_6 transitions. The main peak has the same shape and peak positions agree, but the amplitudes differ. The next two experimental shoulders agree in positioning with theory, but the theoretical structure looks somewhat different. The Σ peak at 7.67 eV could also be the cause of the 7.60-eV experimental shoulder. The bands did flatten somewhat at Γ to produce a broader valley at 7.9 eV, but it did not duplicate the experimental peak at 7.8 eV.

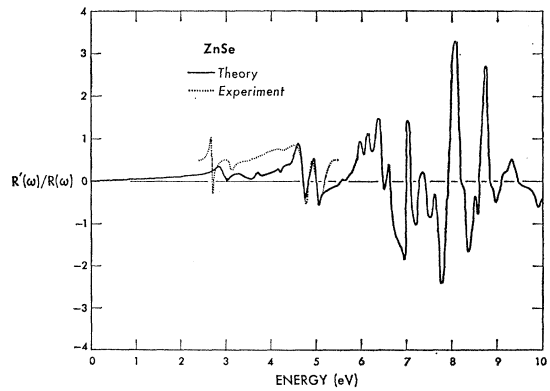

FIG. 8. Comparison for ZnSe of theoretical $R'(\omega)/R(\omega)$ with thermoreflectance measurements by Matatagui *et al.* (Ref. 7). The experimental measurements are multiplied by a constant scale factor.

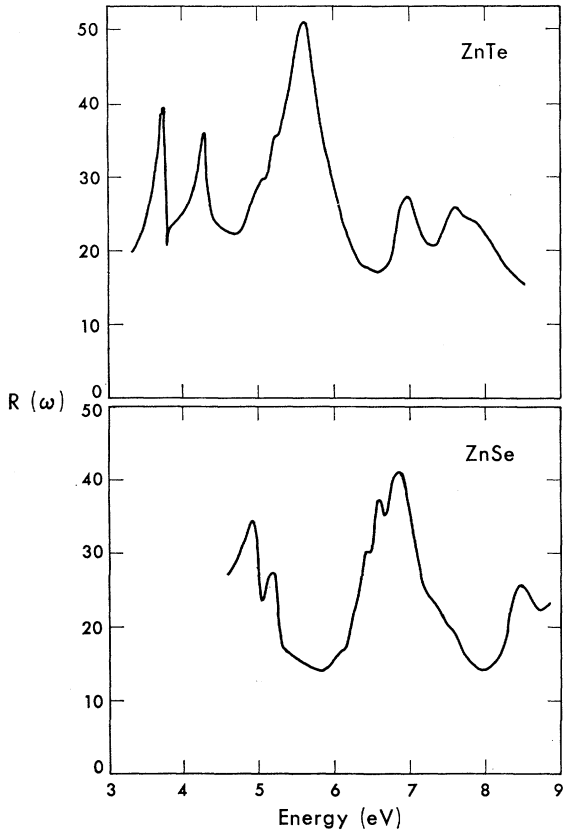

FIG. 9. Experimental reflectivity (percent) for ZnTe and ZnSe at 15°K.

The identifications in the region 8.0 to 10.0 eV are speculative because the shapes of the experimental and theoretical peaks do not agree. The experimental $R(\omega)$ structures at 8.28 and 8.46 eV are attributed to volume transitions near L from bands 7 and 8 to bands 11 and 12. The experimental structures at 8.97 and 9.25 eV are attributed to volume transitions centered at (0.6,0.5,0.2) from bands 5 and 6 to bands 11 and 12. The experimental peak at 9.7 eV is attributed to volume transitions centered at (0.5,0.2,0.1) from bands 5 and 6 to bands 13 and 14.

The agreement between theory and experiment is excellent between 4.2 and 7.8 eV. The agreement becomes progressively worse for higher energies.

A comparison of $R'(\omega)/R(\omega)$ and thermoreflectance data appears in Fig. 8.

C. Low-Temperature Reflectivity

The reflectivity for ZnTe and ZnSe at 15°K (Fig. 9) differs in several respects from the room-temperature reflectivity. Certain of the peaks are greater in magnitude; all peaks are positioned at higher energies and the resolution of the spectrum is slightly better. For both crystals the Λ doublet is much sharper and larger in magnitude at low temperatures. This phenomenon occurs in other similar semiconductors such as GaAs, GaSb, InAs, InSb, and Ge.[15] The Λ doublet is significantly greater in amplitude than it is possible to achieve in the theoretical calculations. This low-temperature sharpening is thought to be caused by exciton effects. Moreover, electroreflectance line shapes also indicate exciton effects at Λ.[16] Thus, the sharpening of the Λ doublet may be explained in terms of the reduction of lifetime broadening of the hyperbolic excitons associated with Λ. No other clear evidence of exciton effects can be seen in the reflectivity. The Σ peaks do become slightly larger at low temperatures, but the sharpening is not sufficient to indicate the presence of excitons.

The general increase in the energies of the reflectivity peaks at low temperature can easily be explained in terms of contraction of the lattice and the Debye-Waller effect. Both of these effects cause the effective electronic potential to become stronger at low temperatures, which causes the spacing between energy bands to increase and the positions of the peaks to shift to higher energies.

For GaAs, we have shown[8] that the temperature dependence of the Λ-doublet peak and the major Σ peak can be calculated accurately from a knowledge of the lattice expansion coefficient and the Debye-Waller factors. Since both ZnTe and ZnSe are in many respects similar to GaAs, we expect that the temperature dependence observed in the present measurements can be accurately explained by similar calculations.

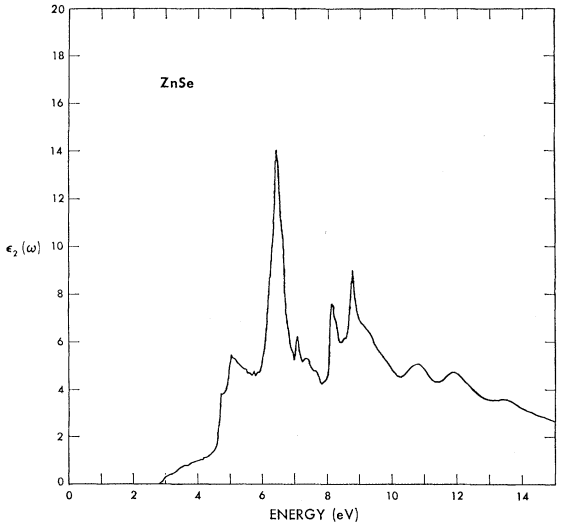

FIG. 10. Composite $\epsilon_2(\omega)$ of direct transitions from 0 to 6.4 eV, of indirect transitions from 12.0 to 14.0 eV and of a linear combination of direct and indirect transitions from 6.4 to 12.0 eV.

[15] R. R. L. Zucca and Y. R. Shen (unpublished); D. L. Greenaway and M. Cardona, in *Proceedings International Conference on the Physics Semiconductors, Exeter* (The Institute of Physics and the Physical Society, London, 1962), p. 666.

[16] K. L. Shaklee, J. E. Rowe, and M. Cardona, Phys. Rev. **174**, 828 (1968).

Finally, slightly better resolution is possible at low temperatures because of decreased phonon emission and absorption. The lifetime broadening is reduced from about 0.15 eV at room temperature to about 0.05 eV at low temperatures.[15] Consequently, in the low-temperature data for ZnTe a new shoulder appears at 5.23 eV, which corresponds to the shoulder at 5.25 eV in the theoretical calculation. For ZnSe, the only significant change in structure is the splitting of the major Σ peak, causing it to agree closely with the shape of the theoretical peak.

III. DISCUSSION

We have obtained good agreement between measured and calculated reflectivity and between $R'(\omega)/R(\omega)$ and thermoreflectance. The agreement appears good enough to indicate that our identifications of the important optical structures are substantially correct and that our band structure is accurate in the region near the fundamental gap.

Significant disparity between experimental and theoretical reflectivity occurs for higher-energy transitions, typically for transitions with energy greater than 2.5 to 3 times the fundamental gap. As pointed out in Ref. 4, this disparity results essentially because of the rapidly decreasing $\epsilon_2(\omega)$ at these energies. In addition, a comparison of the experimental and calculated values of the static dielectric constant reveals that the calculated value is usually 10 to 20% lower than the experimental value, indicating that the $\epsilon_2(\omega)$ contributions are again too low. However, the inclusion of many-body effects has been shown to increase $\epsilon_2(\omega)$ at higher energies.[17] Bardasis and Hone suggest that the dominant scattering process for a high-energy conduction electron is an Auger-type effect, i.e., a two-electron process that need not conserve momentum. The threshold for this type of scattering is approximately twice the fundamental gap.

We attempt to account for these many-body effects with a simple model for adding contributions from indirect transitions at energies greater than twice the fundamental gap. We define a function

$$I(\omega)=\frac{A}{\omega^2}\int_0^{\omega} D(\omega')D(\omega'-\omega)d\omega',$$

[17] A. Bardasis and D. Hone, Phys. Rev. **153**, 849 (1967).

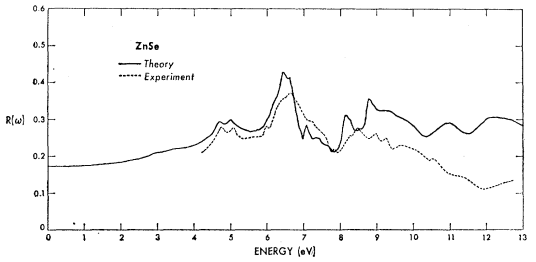

FIG. 11. Theoretical reflectivity is calculated from $\epsilon_2(\omega)$ shown in Fig. 10. The experimental $R(\omega)$ is due to Petroff and Balkanski (Ref. 5).

where $D(\omega)$ is the electronic density of states with the top of the valence band defined as $\omega=0$. A is a normalization factor, defined such that the Kramers-Kronig transform of $I(\omega)$ yields the experimental value of the static dielectric constant. $I(\omega)$ can be interpreted to be the imaginary part of the dielectric function for indirect transitions. For the case of ZnSe, we take the static dielectric constant to be 5.9 and define a new $\epsilon_2(\omega)$:

$$\begin{aligned}\epsilon_2(\omega)&=\epsilon_2(\omega), \quad \omega\leq 6.4 \text{ eV}\\ &=[(12.0-\omega)\epsilon_2(\omega)+(\omega-6.4)I(\omega)]/5.6,\\ &\qquad\qquad 6.4 \text{ eV}\leq\omega\leq 12.0 \text{ eV}\\ &=I(\omega), \quad 12.0 \text{ eV}\leq\omega\leq 14 \text{ eV}\\ &=\beta\omega/(\omega^2+\gamma^2)^2, \quad \omega\geq 14 \text{ eV}.\end{aligned}$$

In other words, we let $\epsilon_2(\omega)$ change linearly from entirely direct transitions at 6.4 eV (about twice the fundamental gap) to entirely indirect transitions at 12.0 eV. A tail function[10] is added at 14 eV.

The resulting $\epsilon_2(\omega)$ and $R(\omega)$ are shown in Figs. 10 and 11. This new $\epsilon_2(\omega)$ is larger at high energies, and this has two desirable effects. First, the calculated static-dielectric constant is raised from 4.7 to its experimental value of 5.9. The second consequence is that the agreement between experimental and calculated reflectivity is much better at higher energies, although some agreement is sacrificed at lower energies.

ACKNOWLEDGMENTS

Two of us (J. P. W. and M. L. C.) thank Dr. T. K. Bergstresser and Dr. S. Bloom for supplying the details of their computer program. We also thank R. N. Cahn for computing values of the orthogonalization integrals.